PAPER

Dimeric anthracene-based mechanophore particles for damage precursor detection in reinforced epoxy matrix composites

Materials Research Express

PAPER

Dimeric anthracene-based mechanophore particles for damage precursor detection in reinforced epoxy matrix composites

Elizabeth M Nofen, Jason Wickham, Bonsung Koo, Aditi Chattopadhyay and Lenore L Dai

School for Engineering of Matter, Transport and Energy, Arizona State University, Tempe, AZ 85287, USA

E-mail: lenore.dai@asu.edu

RECEIVED
2 September 2015

REVISED
19 November 2015

ACCEPTED FOR PUBLICATION
3 February 2016

PUBLISHED
24 February 2016

Keywords: mechanochemistry, mechanophore, dimeric anthracene, epoxy composites, stress sensing

Supplementary material for this article is available online

Abstract

The problem of catastrophic damage purveys in any material application, and minimizing its occurrence is paramount for general health and safety. We have successfully synthesized, characterized, and applied dimeric 9-anthracene carboxylic acid (Di-AC)-based mechanophore particles to form stress sensing epoxy matrix composites. As Di-AC had never been previously applied as a mechanophore and thermosets are rarely studied in mechanochemistry, this created an alternative avenue for study in the field. Under an applied stress, the cyclooctane-rings in the Di-AC particles reverted back to their fluorescent anthracene form, which linearly enhanced the overall fluorescence of the composite in response to the applied strain. The fluorescent signal further allowed for stress sensing in the elastic region of the stress–strain curve, which is considered to be a form of damage precursor detection. Overall, the incorporation of Di-AC to the epoxy matrix added much desired stress sensing and damage precursor detection capabilities with good retention of the material properties.

1. Introduction

Mechanochemistry is the area of research that involves the use of mechanical force to induce a chemical change, with recent study focusing on directing the mechanical force to embedded mechanophore units for a targeted chemical response [1–3]. Mechanophores are molecular units that provide a measureable signal in response to an applied force, often in the form of a visible color change or fluorescent emission [4, 5]. Mechanochemistry additionally offers the materials chemist alternative routes to obtain desired products, as the use of mechanically active groups can allow for reaction pathways not possible with traditional thermal or light-driven reactions [6]. Spiropyran has been previously employed as a mechanophore in elastomeric or thermoplastic systems, undergoing a reversible electrocyclic ring opening reaction under tension to go from colorless to the colored merocyanine form [7–9]. Additionally, cyclobutane [10–15] and cyclopropane [16, 17] have been used as mechanophores, due to the strained nature of the rings, allowing for their easy fracture under force. In a few recent studies, anthracene moieties have also been used as mechanophore precursors, as they have a much higher absolute fluorescence quantum yield compared to other mechanophores, and a large conjugated system, which brings the excitation/emission to longer wavelengths [18]. Anthracene derivatives can form a variety of mechanochemically active species including strained Dewar isomers [19], two cyclobutane rings via [4 + 4] cycloaddition [20], Diels–Alder adducts [21], and cyclooctane rings [22]. However, these derivatives have previously only been studied in solution, films, or elastomers. Besides being used as mechanophores, cycloaddition of anthracene moieties has also been used for shape memory [23] and self-healing applications [24].

The problem of catastrophic damage purveys in any material application, and minimizing its occurrence is paramount for general health and safety. Thus, the ability to sense applied damage and correlate it with a measurable signal is extremely desirable. The use of mechanophores can allow for novel damage detection

schemes through their ability to act as stress sensors in various polymer matrices [25, 26]. It is worthwhile to note that the previously mentioned work on spiropyran, cyclobutane/cyclopropane, and anthracene as mechanophores exclusively involve solutions, thin films, or elastomeric/thermoplastic matrices. There has been limited study of mechanochemistry within the other branch of polymer chemistry, that being thermoset networks. Recently, we have begun to focus on applying mechanochemistry to thermoset composite systems, creating self-sensing polymer blends of cyclobutane-based mechanophores and epoxy in our previous work [27]. In current work, we sought to study a new mechanophore chemistry in epoxy matrices while additionally enhancing the overall damage detection capability and creating a self-sensing mechanophore particle reinforced composite (PRC), rather than a simple polymer blend.

PRCs are ubiquitous for overall property enhancement in a wide variety of applications including microelectronics packages [28], polymer electrolyte membrane fuel cells [29], and the aerospace, automotive, and construction industries [30], due to the virtually unlimited combination of matrix and particles, and the wide variety of particle types and properties. Additionally, the interfaces between the particles and the matrix in PRCs can allow for unique functionalities including the conversion between heat and electricity to create thermoelectric materials [31, 32] and for unique organic−inorganic hybrid solar cells featuring a conjugated polymer matrix and nanocrystal particles [33]. Thus, we desired to create PRCs with dimerized 9-anthracene carboxylic acid (Di-AC) mechanophore particles embedded in an epoxy matrix. To the authors' knowledge, there has only been one other article reporting mechanophore-based particles, in which maleimide−anthracene cycloadducts were attached to silica nanoparticles via poly(methyl acrylate) chains, and were activated via sonication in solution [34]. Additionally, spiropyran-based particles have been synthesized, but they have not yet been tested for mechanical responsiveness, only light and temperature responsiveness [35–37]. Our use of pure mechanophore particles embedded in an epoxy matrix thus elevates the science to a more applied form, and provides facile generation of the stress sensing particles. Thus, we have successfully synthesized, characterized, and applied dimeric anthracene (Di-AC)-based mechanophore particles to form stress sensing particle reinforced epoxy matrix composites. Under an applied stress, the cyclooctane-rings in the Di-AC particles revert to their fluorescent anthracene monomeric form, enhancing the overall fluorescence of the composite, thus adding a sensing capability with good retention of the material properties. This additionally marks the first use of the simple dimer Di-AC as a mechanophore. The resulting fluorescent signal has been found to have a linear correlation with the applied strain, and has further allowed for stress sensing in the elastic region of the stress–strain curve, which is considered to be a form of damage precursor detection.

2. Experimental section

2.1. Materials

9-anthracene carboxylic acid (AC, Alfa Aesar), tetrahydrofuran (THF, Alfa Aesar), 1-methyl-2-pyrrolidinone (NMP, Sigma Aldrich), and deuterated dimethyl sulfoxide (DMSO-d_6, Cambridge Isotope Laboratories) were used as received. The epoxy resin FS-A23 (digycidylether of bisphenol F, DGEBPF) and epoxy hardener FS-B412 (diethylenetriamine, DETA) were purchased from Epoxy systems Inc. and used as received.

2.2. Synthesis and characterization of Di-AC

2 g of AC was dissolved in 40 ml of THF and the mixture was homogenized via magnetic stirring, under a nitrogen purge, and put into darkness. The solution was then photoirradiated with a 302 nm wavelength UV lamp (UVP, UVM-28), with a light density of approximately 1300 μW cm^{-2} at a distance of 3 cm, for three days. A precipitate formed, which was washed with THF by gravity filtration to remove the yellow AC monomer, until the bottom solution was clear. The product was then dried to remove excess solvent. The Di-AC product was obtained as a white powder with a yield of 37%. To ensure the uniformity of the particle size, the Di-AC product was then filtered through 10 μm filter paper (EMD Millipore) with acetone, to gather particles under 10 μm. The particles were allowed to settle and the acetone was decanted off, with subsequent drying of the particles to remove any excess solvent. ^{1}H nuclear magnetic resonance (NMR) spectra were taken with a Bruker 400 MHz NMR spectrometer. The ^{1}H NMR spectra for AC and Di-AC can be found in the supporting information (figures S1 and S2). For the NMR samples, approximately 5 mg of each sample was dissolved in 750 μL of DMSO-d_6. Fourier transform infrared (FTIR) spectra were taken of the pure powder in the ambient atmosphere with a Nicolet iS50 FTIR Spectrometer, with the full spectra found in the supporting information (figure S3). Transmitted light images of the Di-AC powder were taken with a Leica SP5 confocal laser-scanning microscope. The particle size of a dilute solution of 6 mg Di-AC in 5 ml THF was determined via dynamic light scattering (DLS) with a PSS NICOMP 380 ZLS. A Perkin Elmer Lambda 18 UV–visible (UV–vis) spectrometer was used to gather absorption data at ambient for a dilute solution of 1 mg AC in 20 ml NMP before photoirradiation and

after photoirradiating the reported times. The chemical structures of AC and Di-AC were drawn with MarvinSketch.

2.3. Preparation and characterization of mechanophore-embedded epoxy matrix composites

To form the studied composites consisting of 5 wt% Di-AC particles in an epoxy matrix, 0.25 g of the 10 μm filtered Di-AC particles were added to 3.74 g of epoxy resin. These were then mixed with a small impeller mixer at 200 rpm for 10 min at room temperature and checked for the particles to be well dispersed. 1.01 g of the epoxy hardener was then added (to form 5 g total of epoxy at a mass ratio of M_{Resin}: $M_{\text{Hardener}} = 100{:}27$), and mixed with the impeller mixer at 200 rpm for 5 min at room temperature. After the mixture was homogenous, it was poured into silicone rubber molds sprayed with a mold release agent and allowed to cure overnight at room temperature. Neat epoxy samples were prepared in a similar manner with the same 100:27 ratio of resin to hardener. After simple machining, the average dimensions of the samples for the compression test were $3 \times 4 \times 8$ mm and $2 \times 12 \times 35$ mm for the dynamic mechanical analyzer tests. Emission spectra were collected with a Horiba Scientific FluoroLog-3 Spectrofluorometer with an excitation wavelength of 350 nm, with quartz coverslips for the powder samples, and all slits set at 1 nm. A TA Instruments Q20 differential scanning calorimeter was used to determine the glass transition temperature (T_g) of the epoxy samples in aluminum Tzero pans with lids under nitrogen, with air (an empty pan and lid) used as the reference. The sample was first heated to 70 °C to eliminate any thermal history, cooled down to −20 °C, then heated to 120 °C to determine the T_g, with all heating and cooling rates set at 10 °C min^{-1}. A TA Instruments thermogravimetric analyzer Q500 was used to determine the decomposition temperatures (T_d) under nitrogen. Each sample was placed in a tared platinum crucible and heated from 25 °C to 600 °C at a heating rate of 10 °C min^{-1}. A TA Instruments Q800 dynamic mechanical analyzer was used to measure the storage modulus, loss modulus, and tan delta for the epoxy samples over a temperature range and to calculate the crosslink density. The multi-frequency/strain method was used with the single cantilever clamp and a frequency of 1 Hz under amplitude control. The temperature was ramped from 25 °C to 120 °C at a heating rate of 5 °C min^{-1}, with the strain amplitude set at 25 μm. The characteristic temperatures and moduli values were found using the built in functions in the TA Instruments universal Analysis software. A TestResources 800L compression test system was used to compress the samples to different strains and obtain stress–strain plots for the epoxy samples. A small amount of petroleum jelly was applied to the samples to minimize their friction with the compression plate, and prevent unwanted shearing. The tests were run in displacement control in the longitudinal direction at a loading rate of 1 mm min^{-1} and conducted at room temperature. The fluorescence generation from the compressed epoxy samples was observed under a Nikon Eclipse TE300 inverted video fluorescence microscope, by excitation under 340–380 nm UV light, with a filter cube to capture the emission of light between 435 and 485 nm. All images were taken with a black-and-white camera and with the same intensity of light, gain, and exposure time. The Image J (http://imagej.nih.gov/ij/) software package was used to quantify the fluorescence density of the images taken. Every image was first converted to an 8-bit image and then the 'measure' function was used to calculate the integrated intensity for the selected area of the image; this is through the software taking the sum of the pixel values in the image, and then averaging the density at each point. A UVP UV Transilluminator, Model M-20, with an 8 watt and 302 nm wavelength UV light source was used to take macroscopic pictures of the compression test samples. The 8-bit gray scale fluorescence images from both the fluorescence microscope and the transilluminator were pseudocolored green with ImageJ.

3. Results and discussion

3.1. Photodimerization of AC to form Di-AC

It is well known that 9-substituted anthracene derivatives, including AC, form prominently head-to-tail structures when photodimerized in solution under UV light via [4 + 4] cycloaddition to form a cyclooctane-type ring [38]. A schematic of this reaction to form the Di-AC, which can be recovered as a pure white powder, and can be seen in figure 1(a); the head-to-tail structure being preferred due to steric hindrance between the carboxylic acid side chains during dimerization. This dimerization reaction has also been studied in the solid-state, where molecular confinement can allow for the formation of the head-to-head dimer [39, 40]. Additionally, the solid-state [4 + 4] photodimerization phenomenon has allowed for the creation of AC molecular-crystal nanorods that can undergo reversible bending [41, 42]. Figure 1(a) also shows the subsequent incorporation of the Di-AC particles into an epoxy matrix for fluorescent stress sensing via reversion to the AC monomers after stress is applied.

In this study, AC was dissolved in THF and the mixture was homogenized via magnetic stirring, purged with nitrogen, and put into darkness. The solution was then photoirradiated with a 302 nm wavelength UV lamp to carry out the [4 + 4] cycloaddition. The Di-AC white powder precipitate formed, was washed with THF to

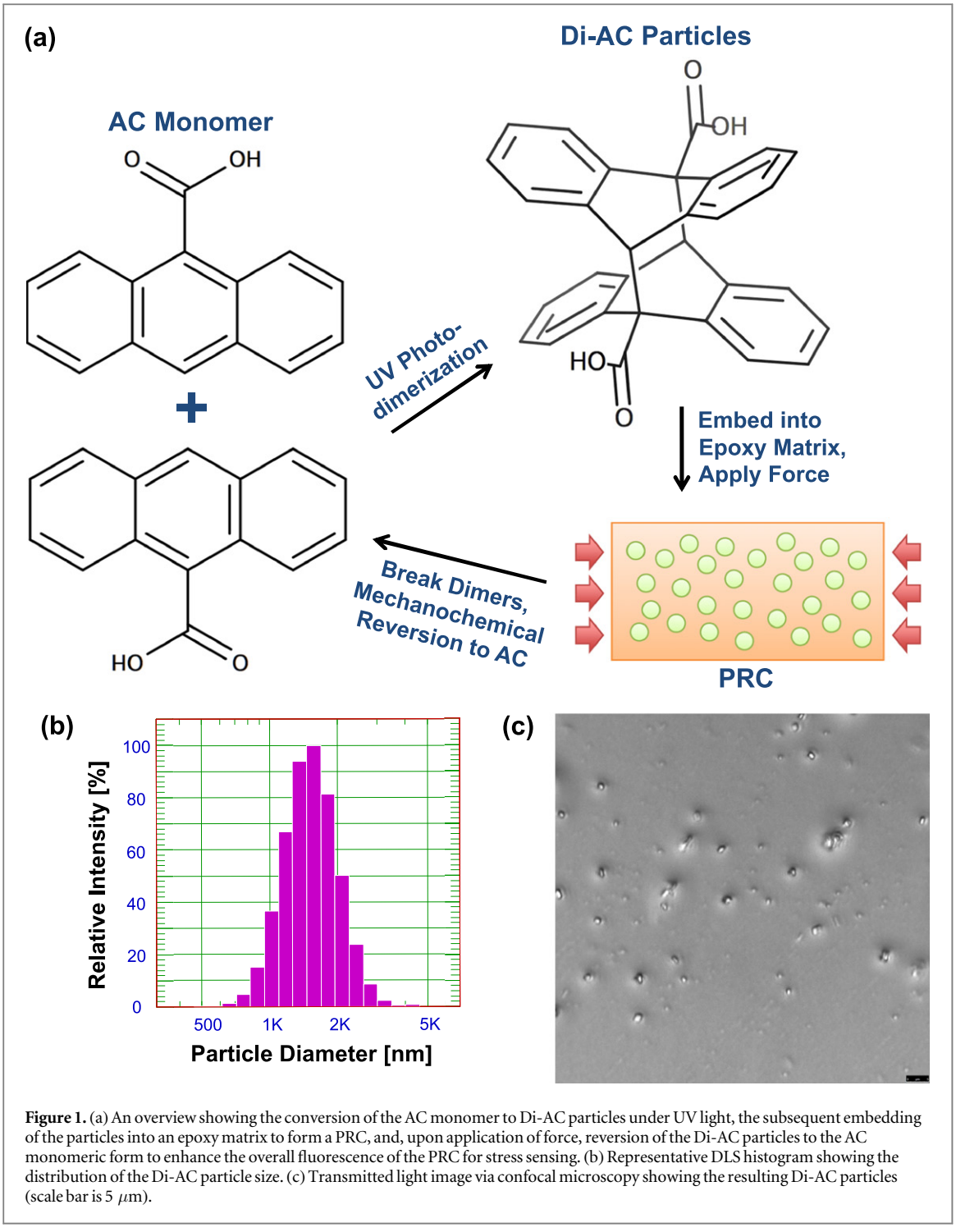

Figure 1. (a) An overview showing the conversion of the AC monomer to Di-AC particles under UV light, the subsequent embedding of the particles into an epoxy matrix to form a PRC, and, upon application of force, reversion of the Di-AC particles to the AC monomeric form to enhance the overall fluorescence of the PRC for stress sensing. (b) Representative DLS histogram showing the distribution of the Di-AC particle size. (c) Transmitted light image via confocal microscopy showing the resulting Di-AC particles (scale bar is 5 μm).

remove any unreacted yellow AC monomer, and dried. After the photodimerization reaction and purification, the resulting Di-AC powder product was filtered through 10 μm filter paper to remove any large aggregates and capture Di-AC particles of a reasonable particle size. DLS was used to confirm the particle size, which was found to be 1553 $\pm$ 739 nm in diameter, with a Gaussian distribution. This distribution can be seen with a corresponding relative intensity graph in figure 1(b). Transmitted light images captured with a confocal laser-scanning microscope confirmed the particle size found from DLS (figure 1(c)).

After confirming the creation of uniform Di-AC particles, the chemistry was also confirmed via NMR and FTIR spectroscopy, comparing AC with Di-AC. The ^{1}H NMR spectra for AC and Di-AC can be found in the supporting information (figures S1 and S2). Both AC and Di-AC showed a peak at 2.5 ppm, which was characteristic to the DMSO-d_6 solvent and a peak at 3.3 ppm that was characteristic of residual water in the sample. For AC, the peaks from 9 to 7 ppm correspond to the aromatic hydrogen atoms on the anthracene ring, with another peak at 13.9 ppm for the hydrogen on the carboxylic acid. For Di-AC, the peaks for the aromatic

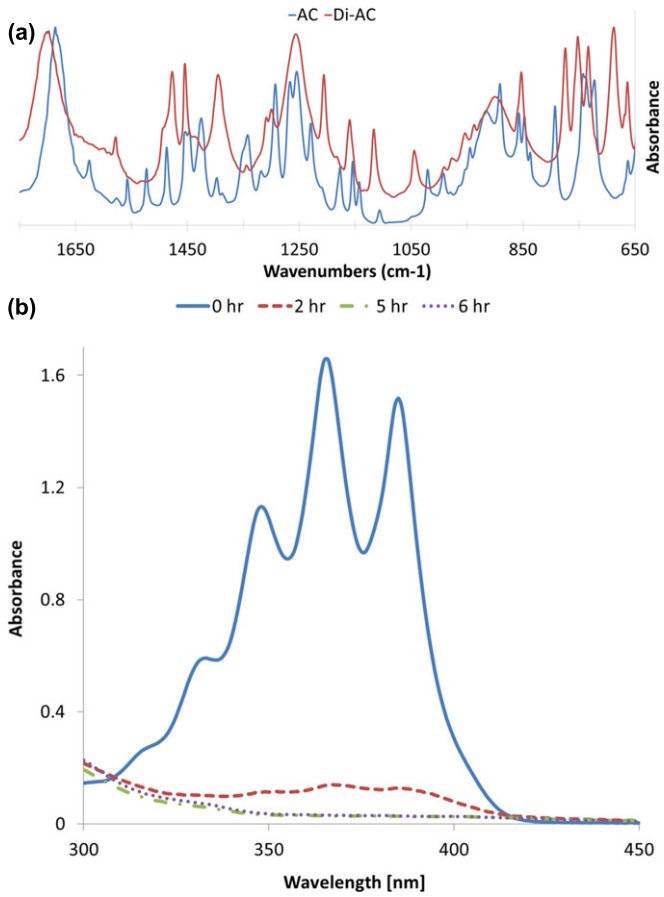

Figure 2. (a) FTIR spectra comparing the unreacted AC monomer with the Di-AC mechanophore product. (b) UV–vis spectra showing the decrease in absorbance over time for a dilute solution of AC in NMP under UV light, with the initial unreacted solution in blue, after 2 h in red, 5 h in green, and 6 h in purple.

hydrogen atoms shifted to 7–6 ppm, the carboxylic acid peak shifted slightly to 13.5 ppm, but the distinguishing peak is at 5.6 ppm, which corresponds to the hydrogen atom on the newly formed cyclooctane ring—confirming the dimerized structure. Figure 2(a) shows the comparison of the FTIR spectra for AC and Di-AC, zoomed in to focus on the characteristic peaks. The full FTIR spectra from 4000 to 400 cm^{-1} can be found in the supporting information (figure S3). There are a few important characteristic peaks in the spectra, the first is for the carbonyl stretch ($\nu_{C=O}$) which blue shifted from 1685 cm^{-1} for AC to 1698 cm^{-1} for Di-AC, indicating a cleavage of some hydrogen bonds when AC transitions to Di-AC and its 3D structure drastically changes [39]. A new sharp peak was formed at 1393 cm^{-1}, corresponding to the newly formed alkane hydrogen (ν_{C-H}) on the cyclooctane ring in Di-AC. Additionally, peaks at 1340 and 1225 cm^{-1} for AC corresponding to the transition band of the phenyl ring were bleached out [39].

The dimerization reaction was further studied by utilizing UV–vis spectroscopy in order to analyze the conversion of AC to Di-AC, as seen in figure 2(b). This analysis is important, as with UV light driven reactions; the addition of light can drive both the forward and reverse reactions, resulting in low conversions. The initial solution (at 0 h) consisted of 1 mg AC in 20 ml NMP, and showed fingerlike absorption bands between 320 and 420 nm, representing vibronic substructures, which are characteristic for anthracene derivatives [39]. 302 nm UV light was applied to the solution and samples were taken at 2, 5, and 6 h to probe the change in the absorbance over time. After 2 h photoirradiation, the absorbance value decreased drastically, with the conversion for the peak at the 365 nm wavelength being 0.92. With the longer application of light, the conversion for the 365 nm peak leveled off at 0.98 for 5 and 6 h. The conversion never reaches 1, as some percentage of the dimers are driven back to the monomeric form under UV light, as previously mentioned. However, 0.98 is a very high conversion for this type of reaction, and is likely due to the relatively small size of the dimers and their freedom to move in the dilute solution. Additionally, after the dimerization occurs to produce the Di-AC needed for the composites, the very small amount of unreacted AC remaining is easily washed out, resulting in a quite pure product. This is an important result, as the mechanical sensing function of the Di-AC works by reversion to the AC monomer, so if there were many AC molecules incorporated in the epoxy before stress is applied, the sensing signal may have been confounded.

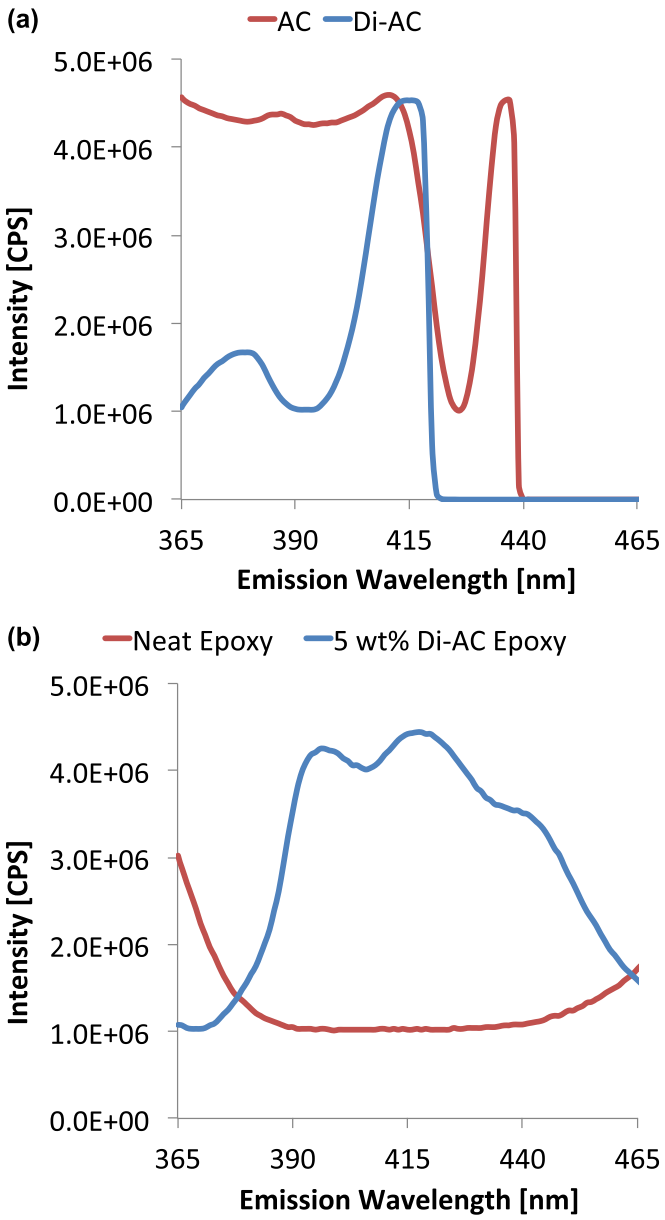

Figure 3. (a) Emission spectra of AC (red) and Di-AC (blue) for an excitation wavelength of 350 nm. (b) Emission spectra of neat epoxy (red) and epoxy embedded with 5 wt% Di-AC for an excitation wavelength of 350 nm.

As the sensing action of the Di-AC mechanophore involves fluorescent emission, it is important to generate emission curves to determine where the emission lies. Figure 3(a) shows the comparison of the fluorescent emission for AC and Di-AC under 350 nm excitation. AC has very strong emission between 365 and 415 nm, with an additional peak at 435 nm. In comparison, Di-AC has a small peak at 378 nm, a large peak at 414 nm, after which it drops off sharply. This shows that while AC has more fluorescence in this region, Di-AC has some fluorescence of its own, albeit less. Following this result, we wanted to see how the fluorescence of Di-AC would affect the overall fluorescence of epoxy when it was incorporated into it.

With the confirmed chemistry of the mechanophore through NMR and FTIR, and the confirmed regular particle size from DLS and confocal images, epoxy composites containing 5 wt% Di-AC particles were synthesized. To form the mechanophore-embedded epoxy, the Di-AC powder with an approximate particle diameter of 1.5 μm was impeller mixed with the epoxy resin so that it would be evenly dispersed throughout the composite. The hardener was then impeller mixed into the resin-particle mixture to obtain a mixture that was viscous and a single phase. This was then poured into rubber molds to create the samples for testing and cured at room temperature overnight. The composition of 5 wt% of Di-AC in the composite was chosen, as this was the least amount of mechanophore that could be used to still generate the desired stress sensing signal. The least amount of mechanophore was desired as incorporating the particles into epoxy interrupts the network formed between the resin and hardener when the epoxy cures, impacting the resulting thermal and mechanical

properties of the composite. It is worthwhile to note that this is a very low amount of mechanophore, with other sensing systems requiring 10, 20%, or more to generate measureable signals [22, 27]. Figure 3(b) shows the comparison of the fluorescent emission for neat epoxy and the 5 wt% Di-AC epoxy composite under 350 nm excitation. The neat epoxy showed a low, flat fluorescence value in the 390–440 nm region, while the Di-AC composite showed broad fluorescence in this region. This emission is markedly different to the emission for the pure Di-AC powder. This can be likely attributed to thermal or mechanical stresses which occurred while the epoxy cured around the Di-AC particles, resulting in some activation of the mechanophore to revert back to the more fluorescent AC form. With this in mind, baseline fluorescence values were taken before the epoxy was stressed during the compression tests, and as long as there was a significant increase in the fluorescence compared to the stress, this method of creating the epoxy composites still produces the desired self-sensing result.

3.2. Thermal and mechanical properties of Di-AC particle reinforced epoxy composites

After the more fundamental characterization of the chemistry related to the Di-AC mechanophore, the thermal and mechanical properties of the embedded composite were evaluated in order to determine the effect of adding the mechanophore. Differential scanning calorimetry (DSC) is a commonly used material characterization method to determine the glass transition temperature (T_g) of various samples be comparing the heat flow required to keep the desired sample and a reference sample (usually air) at the same temperature. Representative DSC scans for the neat and Di-AC composite epoxy can be seen in figure 4(a), the T_gs calculated at the step-wise transition in the curves via the built in TA Universal Analysis software. The average and standard deviation values for the T_g over four runs were 55.82 °C ± 1.53 °C for the neat epoxy and 50.06 °C ± 1.36 °C for the composite epoxy, for a difference of approximately 6 °C. This slight decrease in T_g is expected as the incorporation of the particles can disrupt the intrinsic epoxy network, as previously mentioned. The decrease of the T_g by 6 °C is much improved upon over previous work incorporating crosslinked cyclobutane polymers into epoxy via polymer blends, as that depressed the T_g by 17 °C–28 °C [27]. In the previous work, at least 10 wt% of mechanophore was required for sensing, so lowering the weight percent to 5 wt% allowed for a better retention of the material properties. As the current and our previous work are the first incorporating mechanophores into epoxy matrices, it will be interesting to see what work can come out of exploring the stress sensing in this system.

Figure 4(b) shows representative thermogravimetric analysis (TGA) for the samples, with the corresponding differential thermal gravimetry (DTG) curves in the inset left. These tests were run under nitrogen to eliminate weight loss due to oxidation, and thus purely capture the thermal decomposition of the bonds within the epoxy samples. The main decomposition temperatures (T_d) were found via the peaks in the DTG curves, and were 350.18 °C ± 1.73 °C for the neat epoxy and 349.26 °C ± 1.53 °C for the composite epoxy. These values are not statistically different from each other, so it can be said that the addition of the mechanophore did not change the T_d. Additionally, on the DTG curves, a small shoulder for both samples can be seen around 411 °C. It is worthwhile to note that the T_d of the pure Di-AC powder (prior to embedding) was found to be 238.84 °C ± 4.43 °C, with a small shoulder at 302.67 °C ± 2.18 °C. The relatively high T_d of the pure Di-AC likely contributed to its addition not affecting the T_g of the embedded composite.

In addition to DSC, dynamic mechanical analysis (DMA) can be used to determine T_g values, as well as determine the crosslink density of the epoxy samples. The DMA measures the storage and loss moduli of a sample by physically oscillating the sample, the ratio of the two being defined as tan delta (tan δ). When heat is applied to the sample, eventually there will be a peak in the tan δ, representing the T_g. Figure 5 shows representative DMA curves for the neat and Di-AC epoxy, the T_gs values being 65.4 °C ± 0.6 °C and 66.8 °C ± 1.4 °C, respectively. It is worth noting that while the values for the two are quite comparable, the Di-AC composite shows a higher standard deviation compared to the neat epoxy, possibly due to more variation in the sample in terms of location of particles and curing. Interestingly, the 6 °C difference in T_g values found for the DSC results was not present for the DMA results. This is likely due to the fact that the T_g values were gathered from very different methods, purely thermal for DSC and mechanical for DMA. According to the DMA however, the neat epoxy and the mechanophore composite are very similar, which shows good retention of the material properties, even when the sensing feature is added. Additionally, compared to the DSC, the T_g for the neat epoxy is about 10 °C higher for the DMA, and is about 17 °C higher for the Di-AC epoxy. This has been seen previously when comparing the two methods, and is again due to the methods utilizing different mechanisms to determine the values.

DMA can also be used to calculate crosslink density for a given sample, according to the theory of rubber elasticity [43], $\rho_{xl} = \frac{G'}{3RT}$, where ρ_{xl} is the crosslink density expressed in moles of elastically effective network chains per cm^3 of sample, G' is the rubbery plateau modulus, R is the gas constant, and T is the absolute temperature at which the rubbery plateau modulus is determined. The rubbery plateau modulus is defined where the storage modulus curve flattens out after the T_g is reached, and was 4.42 MPa at 89.0 °C for the neat

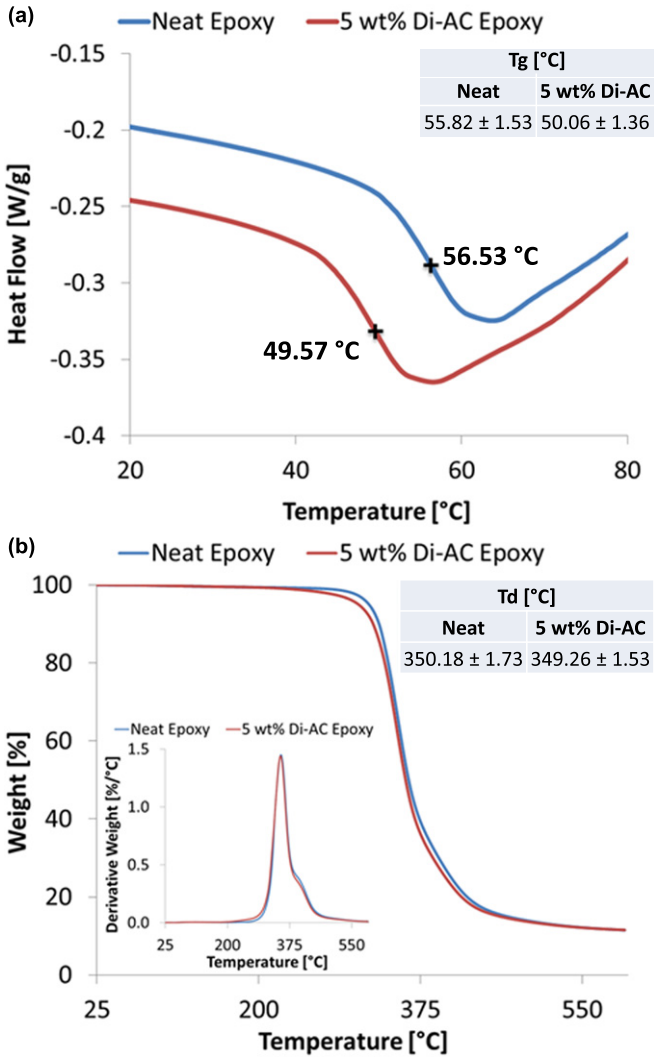

Figure 4. (a) Representative DSC scans showing the glass transition for neat epoxy (red) and the 5 wt% Di-AC epoxy composite (blue), with the resulting T_g values (as an average of four runs) inset on the bottom left. (b) Representative TGA curves showing the decomposition of neat epoxy (red) and the 5 wt% Di-AC epoxy composite (blue), with the resulting major T_d values (as an average of four runs) inset on the top right. The inset left shows the respective DTG curves to determine the T_d values.

epoxy and 4.53 MPa at 87.0 °C for the Di-AC epoxy. Utilizing these values and the theory of rubber elasticity, the crosslink densities were calculated to be $0.50 \pm 0.01 \times 10^3$ mol cm^{-3} and $0.50 \pm 0.01 \times 10^3$ mol cm^{-3}. The crosslink density corresponds to how many crosslinks are able to form between the resin and hardener molecules in the epoxy during curing, and theoretically adding the mechanophore should lower the crosslink density due to the particles disrupting the network. However, this was not seen and the values were essentially the same between the neat and Di-AC embedded epoxy samples. Thus for the thermal characterization of the neat and Di-AC composite samples, while the DSC did show a slight difference in the T_g values, the T_g, T_d, and crosslink density values between two from TGA and DMA showed that adding the mechanophore did little to alter the material properties, providing a benefit for Di-AC PRCs as stress sensors.

To apply the damage to the mechanophore-embedded epoxy samples to observe the resulting fluorescent signal, compression tests were performed and stress–strain curves were generated. figure 6 shows the resulting stress–strain curves for both samples. The Young's modulus values in the linear elastic region of the curve were found to be 2.57 ± 0.06 GPa and 2.46 ± 0.06 GPa for the neat and Di-AC epoxy samples, respectively, which were in good agreement of each other. The yield strength values were 102.77 ± 0.28 MPa and 91.22 ± 1.57 MPa for the neat and Di-AC epoxy samples, respectively. The depression of the yield strength can again be attributed to the particles disrupting the epoxy network. The middle right inset of figure 6 is a UV transilluminator picture under UV light of the compression test samples, neat epoxy on the left and Di-AC composite on the right, showing the macroscopic view of the samples. The samples have each been compressed to 15% strain and the bright green color of the Di-AC sample reflects its much higher bulk fluorescent property.

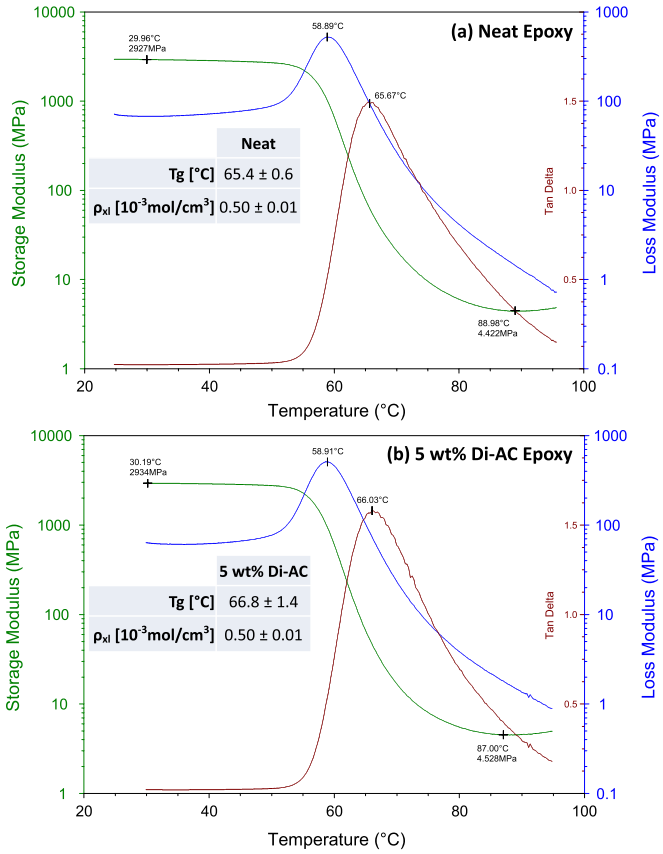

Figure 5. DMA curves showing the Storage Modulus (green), Loss Modulus (blue), and Tan Delta (maroon) of the (a) neat epoxy and (b) 5 wt% Di-AC composite samples, respectively. The inset tables show the average T_g and ρ_{xl} of the samples over four runs, determined from the DMA curves.

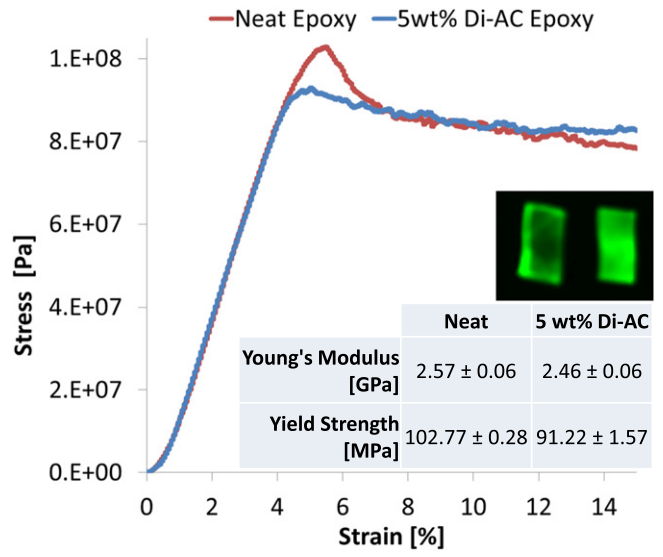

Figure 6. Stress–strain curves for the neat epoxy (red) and 5 wt% Di-AC epoxy (blue), with the lower right inset showing the resulting Young's Modulus and Yield strength values. The inset center right image shows a UV transilluminator picture of the test samples, neat epoxy (left) and epoxy with 5 wt% of Di-AC (right), both compressed to 15% strain. The enhanced fluorescence of the Di-AC epoxy relative to the neat epoxy under UV light can be clearly seen.

3.3. Early damage detection via mechanophore fluorescent signaling

With the full characterization complete for the synthesized mechanophore and mechanophore-embedded composite, its functionality as a stress sensor was evaluated. Compression tests were completed on the

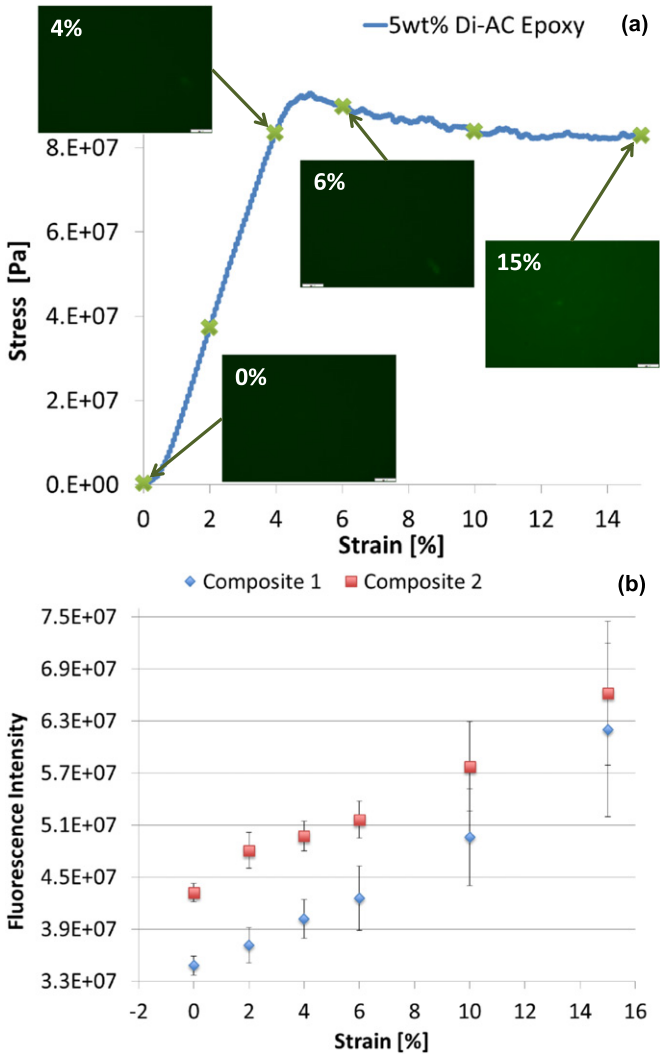

Figure 7. (a) Stress–strain curve for the mechanophore-embedded composite identifying the strain values for which fluorescence images were taken, with representative fluorescence images for 0, 4, 6, and 15% strain. (b) Average fluorescence intensity values for each strain value calculated via ImageJ, with each color representing two separate batches of Di-AC embedded epoxy. Each fluorescence intensity value was averaged over ten pictures for each strain.

mechanophore-embedded composite and at each of the selected strain values; 0, 2, 4, 6, 10, and 15%; ten fluorescence microscopy images were taken representative of the entire sample face in order to quantify any increase of fluorescence. Figure 7(a) shows the locations of the chosen strain values on the stress–strain curve, along with representative fluorescence images for selected strains. The 0% strain is prior to any compression, and provided a baseline for the testing. The 2% strain is clearly in the elastic region, with the 4% strain also being in the elastic region, but right before the yield point. 6% strain is immediately after the yield point, with 10 and 15% strain well into the plastic region. It should be noted that the same testing was performed on the neat epoxy, but no change in fluorescence was observed, as expected.

For each selected strain percentage, the ten fluorescence images were imported into the ImageJ software, and the software calculated average fluorescence intensity values for each image. The values from all ten images were then averaged and plotted with the standard deviations, as seen in figure 7(b). Figure 7(b) shows fluorescence data from two separate batches of the Di-AC embedded composite. It was found that the two separate batches had different fluorescence intensity values initially, but both increased with the strain in a similar way. This shows that Di-AC can be used as a mechanophore in this system, and that applying increasing strain increases the fluorescence emission, due to the breaking of the cyclooctane bonds in the Di-AC particles, causing reversion to the fluorescent monomeric form. Additionally, as the strain was increased, the error bars also increased. We believe this is due to the fact that as the strain was increased, plastic deformation took place in the samples and deformed the surfaces of the epoxy, thus when the fluorescence images were taken, the emission from the mechanophore was altered due to surface roughness. This difference in initial intensity can be due to a number of factors, including the microscope having different light intensity on different days simply due to light source

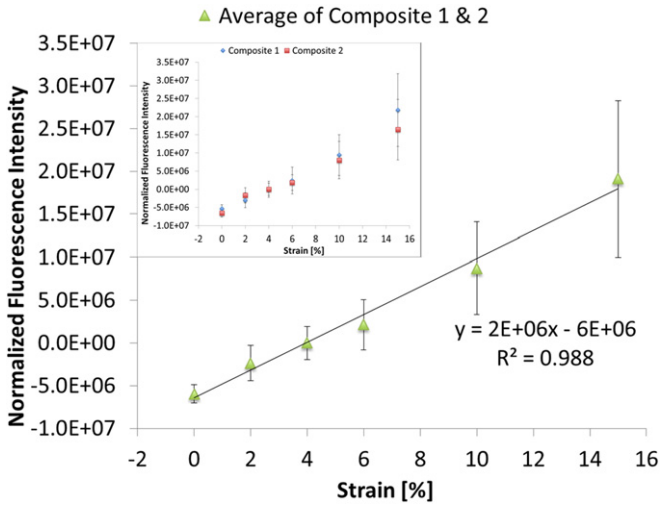

Figure 8. The resulting plot from taking the average intensity of the two composite batches for each strain value, plotted with a linear trendline, with the fluorescence intensity values for the two composite batches (from figure 7(b)) normalized to the 4% strain value, showing the overlaying of the curves in the inset.

ageing, differences in the purity of the Di-AC incorporated, differences in how the epoxy cured and activated the particles, etc.

Regardless, when the data is normalized, the same trend is seen. Figure 8(a) shows the same data, normalized to the 4% strain value. This was done simply subtracting the corresponding 4% average fluorescence intensity value from each strain value, making the 4% strain value 0. Doing this overlays the two curves nicely, showing that even if the samples have different fluorescence initially, the overall trend is still the same. From this curve, it is clear that the 0% and 4% fluorescence values are statistically different. In order to make the curve easier to read, for each normalized strain value the ten images from each batch (20 images total) to create an overall average and overall standard deviation, as seen in figure 8(b). This further highlights the definite statistical difference between 0% and 4% strain, and as seen in figures 7(a), 4% strain is still in the elastic region, which means Di-AC can act as a damage precursor detector. As the region after the yield point in a stress–strain curve corresponds to plastic deformation, where irreparable damage has already taken place, it is ideal to instead achieve the damage precursor detection. In this scheme, a signal alerts to the impending material failure before the yield point (in the elastic region), so the material can be repaired or replaced. For the application of this, if an epoxy part that was incorporated with the mechanophore reached a certain fluorescence value relative to the initial fluorescence, corresponding to 4% strain, it would be known that the part is not damaged yet (it is still in the elastic region), but upon further strain, the yield point would be reached. This is a great improvement to our previous cyclobutane-based mechanophores and epoxy polymer blends, as in that system we were only able to sense damage immediately after the yield point, rather than before [27]. It could be argued that 0 and 2% are also statically different, but there is some overlap of the error bars in the overlayed graph in the inset of figure 8. It was also seen that the 6% intensity value was slightly higher that 4%, with the 10 and 15% values being much higher. Additionally, this characterization of the mechanochemistry is unique in that the fluorescence imaging and resulting analysis allows us to take a look at the microscale signal rather than just macroscale signal popular with visible color change mechanophores.

There has only been one other study on the mechanochemical reversion of these cyclooctane rings formed from the photodimerization of AC back to the monomeric form [22]. Interestingly, that group only reported successful damage detection when the cyclooctane rings were anchored onto connecting poly(vinyl alcohol) chains, and reported no mechanophore property for the pure Di-AC powder, recording no change in the NMR spectra when the powder was ground by hand. Another group that studied the pressure-sensitivity of the strained Dewar isomer of 9-tert-butylanthracene similarly reported no pressure sensitivity for untethered dimeric anthracene [19]. Our hypothesis is that the pure Di-AC particles are held together by hydrogen bonding within the carboxylic acid group, and simple grinding of the mechanophore alone would only break these weaker bonds to form smaller particles through sliding of the particles against one another. This mechanism would thus not allow for sensing, but when the particles are embedded in an epoxy matrix, the thermoset network is formed around the particles, restraining their movement and forcing the cyclooctane rings to be broken under compression. This restraint is thus required for stress sensing with these cycloalkane rings to ensure breakage of the desired bonds.

Additionally, figure 8 shows that a linear fit can be generated for the curve, resulting in a good fit with an R^2 value of 0.988. This implies that with the Di-AC mechanophore embedded in epoxy for stress sensing, a linear relationship can be generated between applied strain or damage and the resulting fluorescence emission, adding another novel feature to this stress sensing scheme.

4. Conclusion

Mechanochemistry is still a relatively new and exciting field, and the pervasive nature of damage makes it an important one. Anthracene moieties make good candidates for mechanophore creation due to their highly fluorescent nature and ease of synthesis. We successfully synthesized, characterized, and applied Di-AC-based mechanophore particles to form stress sensing particle reinforced epoxy matrix composites. As Di-AC had never been applied as a mechanophore on its own previously and thermoset composites are rarely studied for stress sensing, this made for novel work. The particles were found to have a regular 1.5 μm diameter, and the reaction of AC to Di-AC was thoroughly studied via NMR, FTIR, UV–vis, and fluorescence spectroscopy. The 5 wt% Di-AC embedded epoxy composites were further studied with fluorescence spectroscopy, DSC, TGA, DMA, and a compression test. The mechanophore-embedded composites were found to have a slightly lower T_g in the DSC scans, but highly comparable materials properties when studied with the TGA, DMA, and compression test. To apply the damage to the composite samples to observe the resulting fluorescent signal, compression tests were performed and stress–strain curves were generated, with representative fluorescence microscopy images taken at various strain values to observe the increase in fluorescence. Under the applied stress, the cyclooctane-rings in the Di-AC particles reverted back to their fluorescent anthracene monomeric form, which linearly enhanced the overall fluorescence of the composite in response to the applied strain. The fluorescent signal further allowed for stress sensing in the elastic region of the stress–strain curve, which is considered to be a form of damage precursor detection. Overall, the incorporation of Di-AC to the epoxy matrix created a robust composite system with a minor deviation from the mechanical and thermal properties of the neat epoxy, with the much desired added benefit of stress sensing and damage precursor detection.

Acknowledgments

We would like to acknowledge the financial support from the Army Research Office, Grant Number W911NF1510072, Program Manager Dr. David Stepp, and student support from the National Science Foundation Graduate Research Fellowship Program, the ARCS Foundation, and the Fulton Undergraduate Research Initiative. We would also like to acknowledge Dr Bin Mu's Laboratory, the WM Keck Bioimaging Laboratory, the LeRoy Eyring Center for Solid Sate Science, and the Adaptive Intelligent Materials and Systems Center, all at Arizona State University, for facilities use.

References

[1] Silberstein M N, Min K, Cremar L D, Degen C M, Martinez T J, Aluru N R, White S R and Sottos N R 2013 Modeling mechanophore activation within a crosslinked glassy matrix *J. Appl. Phys.* **114** 023504
[2] Black A L, Lenhardt J M and Craig S L 2011 From molecular mechanochemistry to stress-responsive materials *J. Mater. Chem.* **21** 1655–63
[3] Brantley J N, Wiggins K M and Bielawski C W 2013 Polymer mechanochemistry: the design and study of mechanophores *Polym. Int.* **62** 2–12
[4] Potisek S L, Davis D A, Sottos N R, White S R and Moore J S 2007 Mechanophore-linked addition polymers *J. Am. Chem. Soc.* **129** 13808–9
[5] Cho S, Kim J and Chung C 2008 A fluorescent crack sensor based on cyclobutane-containing crosslinked polymers of tricinnamates *Sensors Actuators* B **134** 822–5
[6] Hickenboth C R, Moore J S, White S R, Sottos N R, Baudry J and Wilson S R 2007 Biasing reaction pathways with mechanical force *Nature* **446** 423–7
[7] Celestine A N, Beiermann B A, May P A, Moore J S, Sottos N R and White S R 2014 Fracture-induced activation in mechanophore-linked, rubber toughened PMMA *Polymer* **55** 4164–71
[8] Davis D A *et al* 2009 Force-induced activation of covalent bonds in mechanoresponsive polymeric materials *Nature* **459** 68–72
[9] Gossweiler G R, Hewage G B, Soriano G, Wang Q, Welshofer G W, Zhao X and Craig S L 2014 Mechanochemical activation of covalent bonds in polymers with full and repeatable macroscopic shape recovery *ACS Macro Lett.* **3** 216–9
[10] Cho S, Kim J and Chung C 2010 Photochemical crack healing in cinnamate-based polymers *J. Nanosci. Nanotechnol.* **10** 6972–6
[11] Kryger M J, Ong M T, Odom S A, Sottos N R, White S R, Martinez T J and Moore J S 2010 Masked cyanoacrylates unveiled by mechanical force *J. Am. Chem. Soc.* **132** 4558–9
[12] Kryger M J, Munaretto A M and Moore J S 2011 Structure-mechanochemical activity relationships for cyclobutane mechanophores *J. Am. Chem. Soc.* **133** 18992–8
[13] Chung C, Roh Y, Cho S and Kim J 2004 Crack healing in polymeric materials via photochemical [2 + 2] cycloaddition *Chem. Mater.* **16** 3982–4

[14] Oya N, Sukarsaatmadja P, Ishida K and Yoshie N 2012 Photoinduced mendable network polymer from poly(butylene adipate) end-functionalized with cinnamoyl groups *Polym. J.* **44** 724–9
[15] Cintas P and Cravotto G 2012 Mechanochemistry measuring the force of sound *Nat. Chem.* **4** 77–8
[16] Lenhardt J M, Black A L and Craig S L 2009 Gem-Dichlorocyclopropanes as abundant and efficient mechanophores in polybutadiene copolymers under mechanical stress *J. Am. Chem. Soc.* **131** 10818–9
[17] Ramirez A L B, Kean Z S, Orlicki J A, Champhekar M, Elsakr S M, Krause W E and Craig S L 2013 Mechanochemical strengthening of a synthetic polymer in response to typically destructive shear forces *Nat. Chem.* **5** 757–61
[18] Xing J, Zheng M, Chen W, Dong X, Takeyasu N, Tanaka T, Zhao Z, Duan X and Kawata S 2012 C-2v symmetrical two-photon polymerization initiators with anthracene core: synthesis, optical and initiating properties *Phys. Chem. Chem. Phys.* **14** 15785–92
[19] Tong F, Cruz C D, Jezowski S R, Zhou X, Zhu L, Al-Kaysi R, Chronister E L and Bardeen C J 2014 Pressure dependence of the forward and backward rates of 9-tert-butylanthracene dewar isomerization *J. Phys. Chem.* A **118** 5349–54
[20] Jezowski S R, Zhu L, Wang Y, Rice A P, Scott G W, Bardeen C J and Chronister E L 2012 Pressure catalyzed bond dissociation in an anthracene cyclophane photodimer *J. Am. Chem. Soc.* **134** 7459–66
[21] Yoshie N, Saito S and Oya N 2011 A thermally-stable self-mending polymer networked by Diels–Alder cycloaddition *Polymer* **52** 6074–9
[22] Song Y, Lee K, Hong W, Cho S, Yu H and Chung C 2012 Fluorescence sensing of microcracks based on cycloreversion of a dimeric anthracene moiety *J. Mater. Chem.* **22** 1380–6
[23] Defize T, Riva R, Jerome C and Alexandre M 2012 Multifunctional poly(epsilon-caprolactone)-forming networks by Diels–Alder cycloaddition: effect of the adduct on the shape-memory properties *Macromol. Chem. Phys.* **213** 187–97
[24] Froimowicz P, Frey H and Landfester K 2011 Towards the generation of self-healing materials by means of a reversible photo-induced approach *Macromol. Rapid Commun.* **32** 468–73
[25] Chen Y, Spiering A J H, Karthikeyan S, Peters G W M, Meijer E W and Sijbesma R P 2012 Mechanically induced chemiluminescence from polymers incorporating a 1,2-dioxetane unit in the main chain *Nat. Chem.* **4** 559–62
[26] Ramirez A L B, Schmitt A K, Mahanthappa M K and Craig S L 2014 Enhancing covalent mechanochemistry in bulk polymers using electrospun ABA triblock copolymers *Faraday Discuss.* **170** 337–44
[27] Zou J, Liu Y, Shan B, Chattopadhyay A and Dai L L 2014 Early damage detection in epoxy matrix using cyclobutane-based polymers *Smart Mater. Struct.* **23** 095038
[28] Zhang Z and Wong C 2004 Recent advances in flip-chip underfill: materials, process, and reliability *IEEE Trans. Adv. Packag.* **27** 515–24
[29] Heo S I 2006 Influence of particle size and shape on electrical and mechanical properties of graphite reinforced conductive polymer composites for the bipolar plate of PEM fuel cells *Adv. Compos. Mater.* **15** 115–26
[30] Durand J M, Vardavoulias M and Jeandin M 1995 Role of reinforcing ceramic particles in the wear behavior of polymer-based model composites *Wear* **181** 833–9
[31] He M, Ge J, Lin Z, Feng X, Wang X, Lu H, Yang Y and Qiu F 2012 Thermopower enhancement in conducting polymer nanocomposites via carrier energy scattering at the organic–inorganic semiconductor interface *Energy Environ. Sci.* **5** 8351–8
[32] He M, Qiu F and Lin Z 2013 Towards high-performance polymer-based thermoelectric materials *Energy Environ. Sci.* **6** 1352–61
[33] He M, Qiu F and Lin Z 2013 Toward high-performance organic-inorganic hybrid solar cells: bringing conjugated polymers and inorganic nanocrystals in close contact *J. Phys. Chem. Lett.* **4** 1788–96
[34] Li J, Shiraki T, Hu B, Wright R A E, Zhao B and Moore J S 2014 Mechanophore activation at heterointerfaces *J. Am. Chem. Soc.* **136** 15925–8
[35] Zhu M Q, Zhu L Y, Han J J, Wu W W, Hurst J K and Li A D Q 2006 Spiropyran-based photochromic polymer nanoparticles with optically switchable luminescence *J. Am. Chem. Soc.* **128** 4303–9
[36] Huang C, Wang Y, Hong C and Pan C 2011 Spiropyran-based polymeric vesicles: preparation and photochromic properties *Macromol. Rapid Commun.* **32** 1174–9
[37] Su J, Chen J, Zeng F, Chen Q, Wu S and Tong Z 2008 Synthesis and photochromic property of nanoparticles with spiropyran moieties via one-step miniemulsion polymerization *Polym. Bull.* **61** 425–34
[38] Ito Y and Olovsson G 1997 Use of linker for preparation of missing solid-state photoproducts: head-to-head photodimerization of anthracene-9-propionic acid in its crystalline double salt with cyclohexane-l,2-diamine *J. Chem. Soc.—Perkin Trans.* **1** 127–33
[39] More R, Busse G, Hallmann J, Paulmann C, Scholz M and Techert S 2010 Photodimerization of crystalline 9-anthracenecarboxylic acid: a nontopotactic autocatalytic transformation *J. Phys. Chem.* C **114** 4142–8
[40] Zouev I, Cao D, Sreevidya T V, Telzhensky M, Botoshansky M and Kaftory M 2011 Photodimerization of anthracene derivatives in their neat solid state and in solid molecular compounds *Cryst. Eng. Comm.* **13** 4376–81
[41] Good J T, Burdett J J and Bardeen C J 2009 Using two-photon excitation to control bending motions in molecular-crystal nanorods *Small* **5** 2902–9
[42] Zhu L, Al-Kaysi R O, Dillon R J, Tham F S and Bardeen C J 2011 Crystal structures and photophysical properties of 9-anthracene carboxylic acid derivatives for photomechanical applications *Cryst. Growth Des.* **11** 4975–83
[43] Nielsen L E 1969 Cross-linking-effect on physical properties of polymers *J. Macromol. Sci.—Rev. Macromol. Chem.* **C3** 69–103